Photonic integrated alumina waveguide gratings for far-field structured illumination at UV wavelengths

Chupao Lin,[1,4] **Juan Santo Domingo Peñaranda,**[2] **Jolien Dendooven,**[2] **Christophe Detavernier,**[2] **David Schaubroeck,**[3] **Roel Baets**[1,4] **and Nicolas Le Thomas**[1,4]

[1] *Photonics Research Group , Ghent University-imec*
[2] *Cocoon, Dept. of Solid Stae Sciences, Ghent University*
[3] *Centre for Microsystems Technology (CMST), Ghent University-imec*
[4] *Center for Nano- and Biophotonics (NB-Photonics), Ghent University*
Chupao.Lin@Ugent.be

Abstract: We demonstrate far-field UV structured illumination implemented with integrated aluminum oxide (AlO_x) waveguide gratings. Based on simulation and experimental results, we discuss the performances of two AlO_x waveguide gratings operating at $\lambda = 360\,nm$. © 2021 The Author(s)

1. Introduction

Ultra-violet (UV) light beam engineering is of potential interest for sensing and biological applications. Shaping UV light is however difficult and costly with bulk optics. Such an issue could be solved with photonic integrated circuits (PICs), which have been intensively investigated at infrared wavelengths with the silicon-on-insulator platform and more recently at visible wavelength with silicon nitride, but not at UV wavelengths. Here we investigate the performance of integrated waveguide grating output couplers operating at a wavelength of $\lambda = 360\,nm$ in view of structured illumination microscopy [1] and ion trapping [2]. The waveguide gratings are made of amorphous aluminum oxide (AlO_x) thin films on thermal silicon oxide wafers for large-scale fabrication. In contrast to integrated waveguides [3], gratings operating in the UV wavelength range and compatible with large-scale fabrication have not been reported yet, due to the fabrication challenges related with the typical feature size needed for single mode UV light propagation. We compare the experimental and simulated UV light beam profiles scattered by these UV integrated gratings, and discuss their performance by analyzing the fringe visibility of the interference patterns that they generate in the far-field.

The present PIC that is made of an atomic layer deposited AlO_x thin film consists of a multi-mode interference (MMI) 50:50 beam splitter, two adiabatic tapers and two AlO_x waveguide gratings, as shown in fig. 1(a). A UV laser beam is butt coupled to a 800 nm-wide and 120 nm-thick (h) fully etched single mode alumina waveguide. The waveguide pattern is defined by E-beam lithography and etched by inductively coupled plasma reactive ion etching (ICP-RIE). A splitting ratio of 50:50 in MMI is critical for a high visibility of the interference fringe pattern. Its dimensions are optimized to be $142\,\mu m$ in length and $8\,\mu m$ in width. The waveguide width is adiabatically expanded to $20\,\mu m$ up to the grating input. The grating is formed by partially etching the waveguide with a depth h_e of either 10 nm or 30 nm. Two different grating pitches, $p = 210\,nm$ and $p = 180\,nm$ respectively, are investigated to scatter the UV beam with an angle of $\theta = 11.7°$ and $\theta = 29.3°$, respectively. To minimize scattering loss induced by mode-mismatch at the input of grating, the grating fill factor is designed to be $f = 0.75$. A value > 0.75 can further reduce the loss but leads to an air strip width $< 45\,nm$ for $p = 180\,nm$, which makes the fabrication even more challenging.
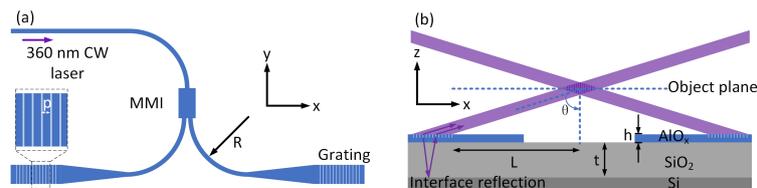

Fig. 1. Schematic of the AlO_x waveguide based photonic integrated circuit: (a) Top view, (b) side view.

2. Simulation and experimental results

The evolution of the scattered beam profile along the beam propagation direction versus the distance L in the horizontal plane, with $L = 0$ located at the grating input, is simulated with a 2D-finite-difference time-domain (FDTD) method in fig 2(a) and (c) for ($\theta = 11.7°$, $h_e = 10\,nm$) and ($\theta = 29.3°$, $h_e = 30\,nm$), respectively. The grating with $h_e = 10\,nm$ exhibits a much lower divergence than for $h_e = 30\,nm$, as a weak grating modulation implies a low coupling efficiency and consequently a low beam divergence. As a result, a larger field of view (FOV) of $170\,\mu m$ is achieved in the first case and a lower FOV of $32\,\mu m$ in the latter. The coupling efficiency is 15.5% for $p = 210\,nm$ and $h_e = 10\,nm$, while a much larger value of 60.4% is obtained for a grating with $p = 180\,nm$ and $h_e = 30\,nm$.

The visibility of the interference pattern generated by the two beams reveals the quality of the symmetry of the scattered beams. Although the intensity of the beam fluctuates partially inside the profile (see fig.2(c)), the visibility is simulated to be as high as 0.97 ± 0.02. The value is higher in the case of $p = 180\,nm$ and $h_e = 30\,nm$, namely 0.99 due to its higher symmetry in a smaller FOV of $32\,\mu m$. The horizontal distance L is fixed at $1.25\,mm$ to provide a convenient off-chip working distance of $1.22\,mm$ for $\theta = 11.74°$ and $1.09\,mm$ for $\theta = 29.3°$.
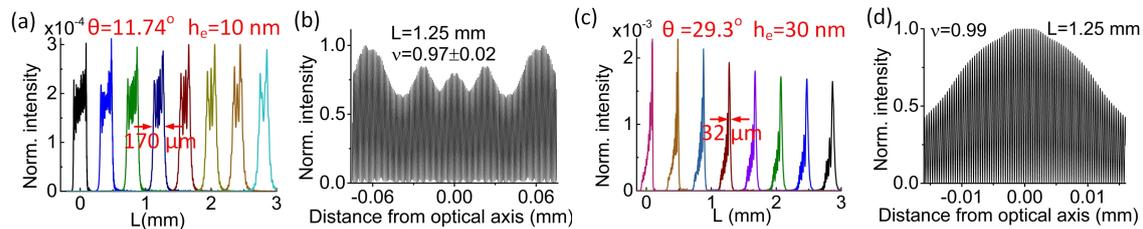

Fig. 2. (a) Scattered beam profile at different distances L for a grating with $\theta = 11.74°$ and $h_e = 10\,nm$, (b) Two-beams interference pattern at a beam intersection corresponding to $L = 1.25\,mm$ in (a). (c) and (d): same as (a) and (b), respectivelly, but for $\theta = 29.3°$ and $h_e = 30\,nm$.

The experimental and simulated near-field and far-field of the beam profile are compared in fig.(3). The experimental intensity decay in the near-filed is slightly faster than the simulated decay profile, due to the presence of propagation losses of the AlO_x waveguide other than the grating scattering loss. The experimental beam profile which is imaged in the the far-field at $L = 1.25\,mm$ matches well simulations. Figure. 3(c) exhibits the experimental interference fringe pattern generated by a pair of gratings with $p = 180\,nm$ and $h_e = 30\,nm$, which is measured with an aspheric lens ($NA = 0.7$). The visibility is estimated to be 0.93 when averaged over a length of $12\,\mu m$.
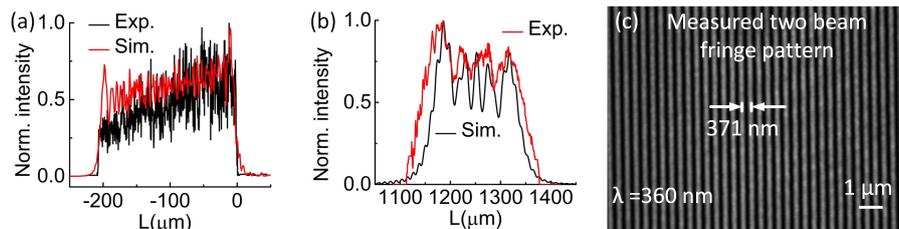

Fig. 3. (a) Near-field and (b) far-field intensity profile of the UV beam scattered by a single grating with $p = 210$ and $h_e = 10\,nm$. (c) Optical image of the far-field interference pattern generated by a pair of gratings with $p = 180$ nm and $h_e = 30\,nm$.

To conclude, the performance of the current UV integrated gratings are relevant for real applications, in particular for structured illumination microscopy.

References

1. R. Heintzmann, T. Huser, Chem. Rev. **117**,13890-13908 (2017).
2. Bruzewicz, C. D., Chiaverini, J., McConnell, R., Sage, J. M. Applied Physics Reviews,**6**, 021314 (2019).
3. West, G.N., Loh, W., Kharas, D., Sorace-Agaskar, C., Mehta, K.K., Sage, J., Chiaverini, J. and Ram, R.J. APL Photonics **4**, 026101-026107(2019).